Comparison of Measurement Methods for 2–150-kHz Conducted Emissions in Power Networks

Deborah Ritzmann, Stefano Lodetti, *Member, IEEE*, David de la Vega, *Senior Member, IEEE*, Victor Khokhlov, *Member, IEEE*, Alexander Gallarreta, Paul Wright, Jan Meyer, *Senior Member, IEEE*, Igor Fernández, and Dimitrij Klingbeil

Abstract—This article presents a comparison of measurement methods for current and voltage distortions in low-voltage networks in the frequency range from 2 to 150 kHz (supraharmonics). The comparison encompasses the methods informatively described in IEC and CISPR international standards, as well as other innovative techniques presented in the literature. This work is carried out within a novel framework that includes advanced and complex synthetic test signals, as well as real grid recordings that allow an accurate comparison of the performance of the tested methods. Specifically designed indices are employed to characterize the accuracy of the tested methods in the frequency and amplitude assessments. In light of that, the strengths and weaknesses of the methods are identified. The results of this article contribute to the ongoing standardization work carried out by the IEC SC77A/WG9 with the purpose of defining a normative measurement method suitable for assessing grid disturbance levels in the range from 2 to 150 kHz.

Index Terms—Harmonics, high-frequency distortion, measurement techniques, power quality, supraharmonics, voltage distortion.

I. INTRODUCTION

MODERN electricity grids are undergoing rapid changes, mainly in the way energy is produced, consumed, and transported. Such evolution, along with several benefits, brings new and unexpected challenges. Among them, the need for ensuring a satisfactory quality of the power supplied has been identified as a crucial requirement for future electricity networks [1]. However, power quality can be compromised by the increasing penetration of power electronic converters, largely employed to connect renewable energy sources

and electric vehicles to the grid, and the improved energy efficiency features of many new household devices (e.g., lighting equipment and induction cookers) [2]–[5].

One of the main concerns is the increasing presence of voltage and current distortions in the frequency range from 2 to 150 kHz, also known as supraharmonic distortion. Despite the relevance of this problem and the attention that it is drawing in the research community, the electromagnetic compatibility (EMC) coordination in this frequency range is still incomplete, mainly due to the lack of a normative field measurement method for compliance assessment of grid disturbance levels. The urgent need for a consistent standardization framework in this frequency range to ensure a satisfactory quality of power supply has already been highlighted [5], and the standardization bodies (e.g., IEC SC77A/WG9) are working in this direction.

This article presents a contribution to this effort by studying the existing measurement methods, contrasting their similarities and differences, and identifying strengths and weaknesses. At present, the relevant standards specify only informative (nonnormative) field measurement methods for assessment of grid compliance [6]–[8]. Comparisons between these measurement methods have been performed and published, discussing the differences in their characteristics, testing them with simple synthetic signals, or comparing their performance with recorded grid signals [9]–[12]. However, in recent years, many efforts have been put into developing alternative measurement methods. New advanced techniques have been published aiming to increase accuracy or reduce computational effort, therefore increasing the range of possibilities [13]–[17]. Thus, there is the need to extend the previous comparisons to include these novel, specifically designed measurement methods for emissions in the 2–150-kHz range.

Building on the framework introduced by the authors in the proceedings article [18], this article presents the results of a comprehensive comparison performed between the currently existing measurement methods for 2–150-kHz emissions in low-voltage (LV) networks. Differences between the methods are highlighted, and their accuracy in identifying and measuring emissions is assessed, setting the grounds for the specification of a suitable new normative method. Moreover, this article recognizes the need for advanced synthetic test signals that can reliably reproduce the specificity of 2–150-kHz emissions as

Method	Center frequencies (kHz)	Number of bins
IEC 61000-4-7	2.1, 2.3, 2.5, …, 149.9	740
IEC 61000-4-30	4, 6, 8, …, 150	74
Digital CISPR 16	2.05, 2.10, 2.15 …, 150.00	2960
Subsampling approach	2.2, 2.4, 2.6, …, 150.0	740
OMP compressive sensing	2.2, 2.4, 2.6, …, 150.0	740
Bayesian compressive sensing	2.2, 2.4, 2.6, …, 150.0	740
Wavelet approach	2.1, 2.3, 2.5, …, 149.9	740

close as possible to real measurements from the LV grid, with controllable parameters and well-defined reference values. A new set of test waveforms is, therefore, employed to improve on the simple sine-wave-based test signals that have been used in previous comparisons and to provide a more representative testing framework.

The rest of this article is structured as follows. In Section II, the methods considered in the comparison are introduced. Section III presents the new framework of test signals, describing how the synthetic test signals are generated based on the features of real signals measured in the grid, and Section IV defines the metrics employed to assess the performance of the tested methods. The results of the comparison are then presented in Section V and discussed in Section VI. Finally, Section VII concludes this article.

II. CANDIDATE METHODS FOR COMPARISON

In addition to the three candidate methods listed in informative Annex C of IEC 61000-4-30, four other methods representative of recent proposals based on nonparametric models are included in this study. The methods differ in various aspects, including the principles used for frequency decomposition, measurement times, and frequency resolution. The third method described in IEC 61000-4-30 Annex C has a frequency resolution of 2 kHz; however, a more granular resolution of 200 Hz is emerging in line with the definition of compatibility levels [19]. The output of all methods is the amplitude values per frequency bin and time interval, which are processed to compute the metrics described in Section IV. The center frequencies associated with the frequency bins of each method are listed in Table I. The rest of this section briefly describes each method considered in the comparison.

A. IEC 61000-4-7

The IEC 61000-4-7 standard defines, in Annex B, an informative method for measuring distortion in the frequency range 2–9 kHz [6] based on a windowed discrete Fourier transform (DFT). A nonoverlapping rectangular window is employed over a measurement interval of 200 ms, i.e., approximately 10/12 power cycles (which is the interval prescribed for harmonics up to 2 kHz for 50 Hz/60 Hz systems). The resulting 5-Hz spaced frequency bins are grouped into 740 final bins each spanning 200 Hz.

B. IEC 61000-4-30

The informative method defined in IEC 61000-4-30 Annex C takes a DFT of 32 windows of length 0.5 ms per

10/12 cycle interval [7]. The gaps between the measurement windows reduce computational cost; however, some emission characteristics could be missed. Since the method has a frequency step of 2 kHz, results are not directly comparable to other methods with a 200-Hz step, but the method is included in the comparison to demonstrate the effect of frequency step on differences in emissions characterization and also to provide a baseline for methods that improve IEC 61000-4-30 by compressive sensing, as described in Section II-E.

C. Digital CISPR 16

Annex C of IEC 61000-4-30 also considers the CISPR 16 standard [8], which specifies instrument characteristics of a measurement receiver for laboratory appliance testing rather than a method for emissions assessment in power networks and leaves room for different digital implementations. A proposal for a compliant implementation for power quality instruments has been made in [20]. The method takes a DFT of overlapping 20-ms windows with a Lanczos shape attenuated to -6 dB at a bandwidth of 200 Hz. The resulting spectra consist of frequency bins spaced 50 Hz apart. The resulting time series of amplitudes for each frequency bin has a time step of 0.5 ms and can be either aggregated or postprocessed by CISPR 16 detectors; the quasi-peak detector is of interest in this study due to its relevance in the definition of compatibility levels in the 9–150-kHz range. The quasi-peak is the maximum of a weighted signal envelope obtained by processing the time series of amplitude values with a cascade of digital filters [21].

D. Subsampling Approach

By the Shannon–Nyquist theorem, a sampling rate of at least 300 kHz is required to measure emissions up to 150 kHz. The subsampling approach has been proposed to enable the use of existing power quality instruments limited to lower sampling rates [13]. An analog filter bank decomposes the input signal into ten bandwidths of 15 kHz, which requires a minimum sampling rate of only 30 kHz. The ten bandlimited, subsampled signals are processed by calculating the DFT of consecutive rectangular 5-ms windows with a correction of the baseband frequencies to reflect the original components of the respective bands.

E. Compressive Sensing

The underlying assumption of compressive sensing is the sparsity of emissions in the frequency domain, meaning that they are well described by a small subset of the 740 frequency bins from 2 to 150 kHz. This subset of components is estimated from 2-kHz bins, and the remaining components are assumed to be zero. A key advantage of compressive sensing is the possibility to decrease the frequency step from 2 kHz to 200 Hz while maintaining a window length of 0.5 ms.

1) OMP Compressive Sensing: A method that uses orthogonal matching pursuit (OMP) as a compressive sensing algorithm has been proposed [14]. The method first processes the input signal with a DFT of consecutive rectangular 0.5-ms

windows to obtain 2-kHz bins. The compressive sensing is based on a multiple measurement vector model to reduce computation time, whereby a sparse estimation is computed simultaneously for a 200-ms block of 400 spectra. For all 400 spectra, the same number of 200-Hz frequency bins is estimated, i.e., the same sparsity is assumed, and it must be estimated in advance.

2) Bayesian Compressive Sensing: In the same way as OMP compressive sensing, this method has no gaps between 0.5-ms measurement windows and also uses a multiple measurement vector model but aims to improve accuracy over OMP by employing sparse Bayesian learning, which determines the joint sparsity automatically [15]. The parameters of the likelihood function and convergence threshold of the iterative algorithm have been set as specified in [15].

F. Wavelet Approach

An alternative to a DFT-based method is wavelet packet decomposition (WPD) of the digitized signal [16]. The WPD recursively filters and downsamples the input signal until a bandwidth of 200 Hz is achieved across the spectrum from 2 to 150 kHz. The filters are as flat as possible, designed to capture 100% of the energy of the frequencies in each bin. The result is a critically sampled signal for each frequency bin, and the amplitude value per measurement interval is calculated by taking the root-mean-square (rms) of the samples. The measurement interval is a rectangular window with a length of ten cycles synchronized to the power system frequency.

III. DESCRIPTION OF TEST SIGNALS

A. Generation of Synthetic Signals

A pivotal role in comparing measurement methods is played by the test signals employed in the analysis. Some previous studies were based on simple single-frequency tones of constant or variable amplitude [10], [12], which is appropriate for assessing the amplitude accuracy of specific frequencies in laboratory conditions, but far from being a faithful representation of the distortion that can be found in power networks. More complex signals, including representative grid recordings, have been utilized [9], [12], but these cannot be used to calculate the accuracy of the methods since their true frequency content is unknown.

This article aims at a deeper and wider analysis, employing specifically designed test signals with theoretical amplitude reference values that are representative of the frequency content of the grid. For this purpose, a set of synthesized test signals has been developed, where center frequency, bandwidth, and amplitude of emissions can be adjusted to be similar to grid recordings. The test signals are defined in terms of power spectral density (PSD), from which the reference levels for spectral amplitudes can be calculated according to the required bandwidth. In this way, the following features of the candidate methods can be studied: amplitude accuracy for signals of different bandwidth (from single-frequency to broadband signals), frequency resolution (both frequency accuracy and discrimination of signals close in frequency), and the impact of method basis (DFT-based, wavelet approach, subsampling,

or compressive sensing). The development of these complex and configurable signals is based on the identification and characterization of the types of emission in the LV grid [4], [22], which are summarized in the following, where the bandwidth is abbreviated as BW.

1) *Narrowband nonintentional emissions (NIEs):* High-amplitude NIEs at discrete frequencies, in the form of tonal and harmonics of tonal emissions ($BW_{-3\,dB} < 1$ kHz), frequently caused by inverters and power electronic converters with switching frequencies operating in the range of tens of kHz [4], [23]. Although the average amplitude is quite stable over time, periodical variations of tens of milliseconds are sometimes observed [4].

2) *Broadband NIEs:* Similar characteristics to narrowband NIEs, but with $BW_{-3\,dB} > 1$ kHz.

3) *Power line communication (PLC):* Nonperiodical short transmissions, based on orthogonal frequency-division multiplexing (OFDM)-modulated bursts in CENELEC-A band [24].

4) *Colored Noise:* Noise of variable amplitude, present in the entire spectrum, generated by different types of motors and electronic devices, usually of higher amplitude at low frequencies [25].

The OFDM-modulated PLC transmissions are created as a combination of sinc functions generated by polar coding. To achieve this, each subcarrier of the OFDM modulation that composes the PLC transmissions is generated following the standard of a commonly used PLC technology (PRIME v1.3.6 [24]). The reference values are calculated by adding the reference values of each subcarrier. Finally, the OFDM signal is bandpass filtered to remove the side lobes generated by the grouping of all the subcarriers. The rest of the synthetic emissions is generated by additive white Gaussian noise (AWGN) and subsequent bandpass filtering.

B. Test Signals for the Comparative Analysis

In order to select a test signal with emissions that are representative of the different types described in Section III-A, several measurement recordings from the LV grid have been considered [4], [22]. Test signal A, shown in Figs. 1 and 2, was selected because it contains not only narrowband but also broadband NIEs, PLC transmissions, and colored noise, which are all commonly found in LV networks. Test signal A was measured in an access point of the LV distribution grid in an urban environment, with a smart metering system in operation in CENELEC-A band. The measurement system was composed of a voltage probe that provides galvanic isolation and protection against transient overvoltages, an oscilloscope for high-resolution sampling (16-bit, 8.92-MHz sampling rate) and a laptop to configure, automatize, and record the measurements [4]. The measurement was recorded with a bandpass filter to remove frequencies outside the range 2–150 kHz. The details of the uncertainty of the measurement system are described in [4] and [26].
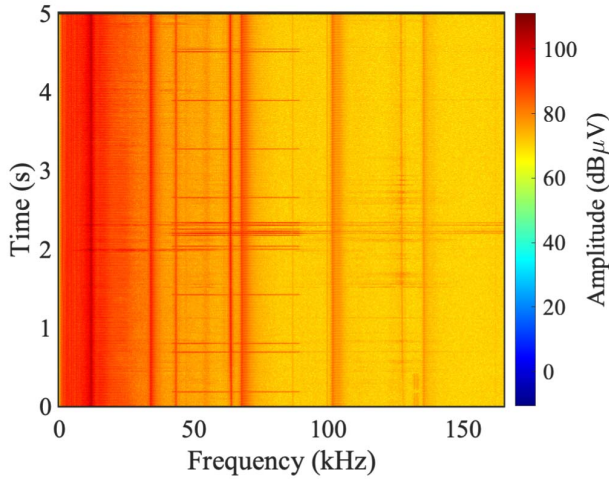
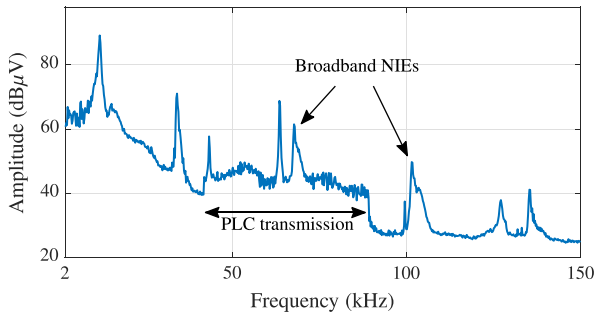Fig. 1.   Spectrogram of the measured grid signal (test signal A).

Fig. 2.   Spectral amplitude for the measured grid signal (test signal A), after applying the IEC 61000-4-7 method, where broadband NIE and PLC bursts are marked. All the nonmarked high-amplitude emissions are narrowband NIEs.

Test signal B is a simple synthesized signal, composed of a single frequency tone of constant amplitude, which is commonly used for calibration.

Test signal C has been generated using AWGN and bandpass filtering to synthesize grid narrowband NIEs at different distances in frequency in order to evaluate challenges related to frequency resolution and identification of close narrowband emissions. The first set of emissions is in the range 33–36 kHz with distances from 300 to 400 Hz; the second set of emissions is in the range 39–46 kHz with distances from 1.2 to 1.4 kHz. The amplitude values are shown in Fig. 3.

Test signal D is a synthesized grid signal generated using AWGN and sinc functions, as described in Section III-A; the amplitude values are shown in Fig. 4. The parameters of the frequency content were based on test signal A to create a signal that is approximately representative of grid emissions, but it must be noted that an exact replication of the grid signal is not possible since there are no known values for amplitudes, frequencies, bandwidth, and duration. The test signal contains narrowband NIEs of different bandwidth, PLC transmissions (the OFDM bursts were estimated in time, duration, and amplitude and then developed according to PRIME standard), and colored noise of amplitude decreasing with frequency. Moreover, variation over time in narrowband NIEs is modeled as a peak-to-peak amplitude deviation of 90%.

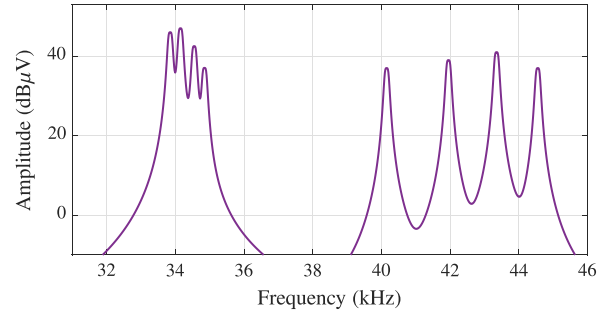The fundamental component and the frequencies below 2 kHz and above 150 kHz can influence the accuracy

Fig. 3.   Synthesized signal with several narrowband emissions (test signal C) and reference level in dBμV for a unit bandwidth (1 Hz).
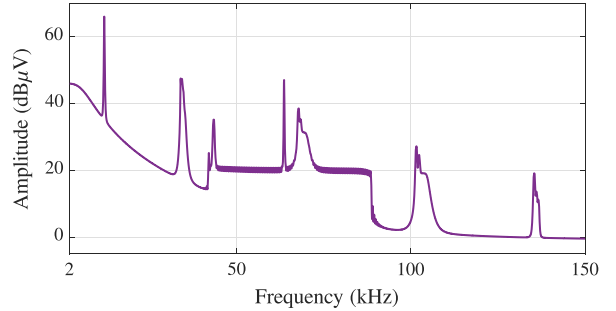

Fig. 4.   Synthesized signal based on the grid recording (test signal D) and reference level in dBμV for a unit bandwidth (1 Hz).

of methods. Most of these frequencies are normally removed by filtering techniques before the methods considered in the study are applied. If the power frequency deviates significantly from 50 Hz, its leakage might occur even at frequencies above 2 kHz and cannot be removed by a high-pass filter. However, under normal operating conditions in interconnected networks, this leakage does not have a significant impact on measurement results. Therefore, the abovementioned synthetic test signals only include frequency components from 2 to 150 kHz.

IV. METRICS FOR ACCURACY ASSESSMENT OF METHODS

A. Reference Values

In this study, candidate methods are compared against reference levels that reflect the thermal impact of emissions over a given bandwidth. Let $G(x)$ be reference values for a unit bandwidth (1 Hz) as a function of frequency x for a given synthetic signal, and then, the amplitude reference value R_f at frequency f for a bandwidth β is calculated as

$$R_f = \sqrt{\sum_{x=f-\beta/2+1}^{f+\beta/2} G(x)^2}. \qquad (1)$$

By this definition, R_f represents 100% of the signal power in the frequency range $[f - \beta/2 + 1, f + \beta/2]$, corresponding to a flat frequency response over the bandwidth β. All reference values in this study have been calculated using $\beta = 200$ Hz in line with the bandwidth of compatibility levels.

B. Amplitude and Frequency

Each method results in amplitudes for frequency components in the range 2–150 kHz reported at regular time intervals. Let variable $U_{b,i}$ be the amplitude value reported for frequency
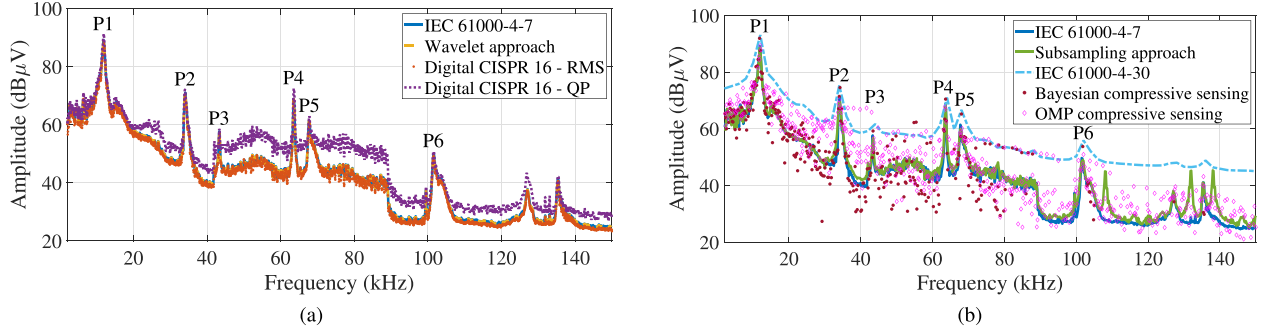
Fig. 5. Spectral amplitude results for the measured grid signal (test signal A). Results have been divided between two figures for visual clarity; values for IEC 61000-4-7 have been included in both figures to enable comparison. (a) Results for the IEC 61000-4-7 method, wavelet approach, and Digital CISPR 16 method. (b) Results for the IEC 61000-4-7 method, subsampling approach, IEC 61000-4-30 method, and compressive sensing methods.

bin b and time interval i. As a representative quantity over the duration of a test signal, the amplitude values $U_{b,i}$ of each frequency bin are aggregated over the number of time intervals N into rms values U_b.

The measurement accuracy for narrowband emissions is assessed by calculating the error in amplitude and frequency of the aggregated rms values identified by each method for characteristic emissions defined in the synthetic signals with known reference values. Let variable U_P be the reference value for the peak amplitude of a given characteristic narrowband emission and f_P the respective frequency value; similarly, let $U_{b,P}$ be the peak amplitude result identified by a given method and $f_{b,P}$ the frequency of the respective bin. Then, the error in frequency $E_{f,P}$ is defined as

$$E_{f,P} = f_{b,P} - f_P \tag{2}$$

and the percentage error in peak amplitude $E_{U,P}$ is defined as

$$E_{U,P} = (U_{b,P}/U_P - 1) * 100. \tag{3}$$

If the magnitude of $E_{f,P}$ does not exceed 50% of the frequency step of a method, then the correct frequency bin has been identified for the peak emission.

C. Integral Value

Integral values are a useful additional measurement quantity for assessing the total power of emissions over a frequency range. Given M adjacent frequency bins with center frequencies $f_m, m = 1, 2, 3, \ldots, M$, the integral value T_{f_1, f_M} is calculated as [12]

$$T_{f_1, f_M} = \sqrt{\sum_{m=1}^{M} U_{f_m}^2} \tag{4}$$

where U_{f_m} is the rms amplitude result for the frequency bin centered at f_m. Let τ_{f_1, f_M} be the integral value calculated from the reference level R_f of a synthetic test signal, calculated as

$$\tau_{f_1, f_M} = \sqrt{\sum_{m=1}^{M} R_{f_m}^2}. \tag{5}$$

Then, the percentage error in the integral value is

$$E_T = (T_{f_1, f_M}/\tau_{f_1, f_M} - 1) * 100. \tag{6}$$

For the CISPR 16 method, the calculation of integral values according to (4) is not suitable without additional compensation for the difference in effective bandwidth relative to the reference level. The method for this compensation is still an ongoing research topic, and no general definition exists; therefore, no integral values are reported for the CISPR 16 method in this article.

V. COMPARATIVE ANALYSIS OF RESULTS

The four test signals introduced in Section III have been processed by the methods in Section II to obtain the metrics defined in the previous section. This section provides a quantitative and qualitative analysis of the results in order to compare the methods with respect to different types of characteristic emissions. First, the range of results between methods for the real signal measured in the LV grid is considered; thereafter, the accuracy of the methods is assessed using the three synthetically generated signals with known reference values. It must be noted that the reported errors in digital CISPR 16 rms values and IEC 61000-4-30 rms amplitudes arise by necessity from the difference in bandwidth definitions to the reference level, rather than intrinsic deficiencies of the algorithms. Since quasi-peak values are a different measurement quantity, error values with respect to rms reference levels are not a useful metric and are, thus, not included in the tables in this section. However, to illustrate the difference compared with rms amplitudes, quasi-peak values have been included in graphical results. The plotted results of the methods for a single signal have been divided between two figures for visual clarity. The values for the error in frequency of peak amplitudes are only reported if they exceed 50% the frequency step of the method, i.e., greater than 25 Hz for digital CISPR 16, 1 kHz for IEC 61000-4-30, and 100 Hz for other methods.

A. Results for the Measured Grid Signal—Test Signal A

Fig. 5 shows the plots of the rms amplitude values for the measured grid signal for all methods, as well as quasi-peak values calculated using the digital CISPR 16 method. It can be seen in Fig. 5(a) that the plots of rms results overlap for the IEC 61000-4-7 method, wavelet approach, and digital CISPR 16, while the quasi-peak values are consistently

TABLE II

RESULTS FOR PEAK NARROWBAND EMISSIONS AND INTEGRAL VALUES FOR THE MEASURED GRID SIGNAL (TEST SIGNAL A)

	Frequency and amplitude of peak emissions												Integral values	
	f_{P1} (kHz)	$U_{f,P1}$ (dB µV)	f_{P2} (kHz)	$U_{f,P2}$ (dB µV)	f_{P3} (kHz)	$U_{f,P3}$ (dB µV)	f_{P4} (kHz)	$U_{f,P4}$ (dB µV)	f_{P5} (kHz)	$U_{f,P5}$ (dB µV)	f_{P6} (kHz)	$U_{f,P6}$ (dB µV)	$T_{40,90kHz}$ (dB µV)	$T_{2,150kHz}$ (dB µV)
IEC 61000-4-7	11.90	89.1	34.10	71.0	43.30	57.7	63.50	68.7	67.70	61.4	101.50	49.7	74.4	94.5
Wavelet approach	11.90	89.2	34.10	71.1	43.30	57.8	63.50	68.7	67.70	61.5	101.50	49.7	74.5	94.6
Digital CISPR 16 - RMS	11.90	88.6	34.05	70.5	43.40	57.1	63.60	68.7	67.80	60.9	101.60	49.2	-	-
Subsampling approach	12.00	88.7	34.20	69.5	43.40	56.8	63.60	68.7	67.80	59.9	101.80	49.0	74.6	94.6
IEC 61000-4-30	12.00	93.1	34.00	75.3	44.00	61.7	64.00	71.0	68.00	66.7	102.00	55.9	74.9	94.2
Bayesian CS[1]	11.80	91.9	34.20	74.6	43.40	59.2	63.60	70.5	68.00	65.2	101.80	53.8	75.3	95.6
OMP CS[1]	12.00	89.3	34.00	70.3	41.60	67.3	63.40	67.7	68.20	60.2	102.00	51.0	77.0	95.1
Range	0.20	4.5	0.20	5.8	2.40	10.5	0.60	3.3	0.50	6.8	0.50	6.9	2.6	1.4

[1] Compressive sensing

higher. Eight peaks of narrowband emission can be clearly distinguished from a decreasing noise level and broadband emission in the PLC region from 40 to 90 kHz. The plots in Fig. 5(b) show a broader range of emission levels and shapes of the amplitude spectrum. Results from the IEC 61000-4-30 method are consistently higher, and the peaks are less distinct from noise as each 2-kHz bin reports the root sum square of ten 200-Hz bins. The subsampling approach results in similar values as the methods in Fig. 5(a), with some additional peaks above 108 kHz. The Bayesian compressive sensing gives a very sparse signal representation, particularly above 90 kHz. Around 80 kHz, it can be seen that, for some frequency components, compressive sensing was not effective in decreasing frequency step from 2 kHz to 200 Hz, as the amplitude values coincide with the levels of the IEC 61000-4-30 method.

Table II lists the results for peak amplitude and frequency values identified by the different methods for six of the characteristic narrowband emissions. It can be observed that there is strong agreement in the frequency value of the first two peaks, with a range of only 200 Hz, while there is more discrepancy in the frequency values of other peaks, mainly due to the IEC 61000-4-30 and compressive sensing methods. The difference in peak amplitude values between methods ranges from 3.3 to 10.5 μV, corresponding to a difference of approximately 40%–300% between the reported peak values. The variation in the calculated integral values is lower with 2.6 dBμV for the PLC region and 1.4 dBμV for the total signal power over 2–150 kHz.

Since there is no reference value for the recorded grid signal, no conclusions can be made about the absolute accuracy of the methods. In order to investigate the source of the relative differences in results between methods, the accuracy is assessed in the following sections using synthetically generated signals with known frequency content.

B. Single-Frequency Sine Wave—Test Signal B

The accuracy for the calibration case can be validated by testing the methods with single-frequency sine wave signals of constant amplitude. The frequencies have been selected such that, for each method, there is a case where the signal frequency coincides with a center frequency and a case where the signal frequency is halfway between center frequencies. The reason for the latter case is to demonstrate the variation in frequency response due to the splitting of energy between adjacent bins. For the IEC 61000-4-7 method, this effect is tested by setting the relevant frequency halfway between 5-Hz bins, i.e., 20.0025 kHz.

The results in Table III show the errors in peak amplitude of up to −50%, which occurs for signal frequencies halfway between center frequencies. The error in integral values remains below 1% for the IEC 61000-4-7 method, wavelet approach, subsampling approach, IEC 61000-4-30, and OMP compressive sensing. The absolute amplitude error for the digital CISPR 16 method reaches only 0.6% because of the overlapping response of the frequency bins. The results for the 21-kHz sine wave demonstrate the capability of the Bayesian and OMP compressive sensing methods to decrease the frequency step by reducing error in amplitude compared with the IEC 61000-4-30 method.

Single-frequency sine wave signals provide some insight into the accuracy of the methods, but they are artificial cases, which would rarely be encountered during grid measurement.

C. Several Narrowband Emissions–Test Signal C

The second synthetic signal tests the response of the methods to emissions with nonzero bandwidth as opposed to discrete single-frequency tones. The identification of the shape of the spectrum is relevant for the characterization of the type and source of emissions, while the priority for compliance assessment is to identify the worst emissions, corresponding to the highest emission level. Fig. 6 shows the plots of the amplitude results, including the indications of the highest peak in both frequency ranges. Errors in frequency and amplitude of the highest peak in each frequency range are given in Table IV to assess how well the worst emissions are identified.

Considering the set of emissions with narrow spacing in the range 33–36 kHz, Fig. 6(a) shows that the digital CISPR 16 method traces the spectral shape of the reference level most accurately due to its smaller frequency step, indicating four spectral peaks. For the more widely separated emissions in the range 39–46 kHz, all methods in Fig. 6(c)

TABLE III
ERRORS IN RESULTS FOR SINGLE-FREQUENCY SINE WAVES (TEST SIGNAL B)

Reference frequency	20.0 kHz		20.0025 kHz		20.025 kHz		20.1 kHz		21.0 kHz	
Error (%)	$E_{U,P}$	E_T[1]	$E_{U,P}$	E_T[1]	$E_{U,P}$	E_T[1]	$E_{U,P}$	E_T[1]	$E_{U,P}$	E_T[1]
IEC 61000-4-7	0.0	0.0	−29.5	0.0	0.0	0.0	0.0	0.0	0.0	0.0
Wavelet approach	−28.4	0.1	−1.9	0.1	−0.2	0.1	0.0	0.1	−28.1	0.1
Digital CISPR 16 - RMS	0.0	-	0.0	-	−0.6	-	0.0	-	0.0	-
Subsampling approach	0.1	0.1	0.0	0.0	−2.7	−0.1	−36	−0.1	0.1	0.1
IEC 61000-4-30	0.0	0.0	0.0	0.0	0.0	0.0	−0.4	0.0	−36.3	−0.3
Bayesian compressive sensing	0.0	0.0	0.0	0.0	−12.0	−11.1	−49.8	−29.0	0.0	0.0
OMP compressive sensing	0.0	0.0	0.0	0.0	0.0	0.0	−22.9	−0.4	0.0	0.0

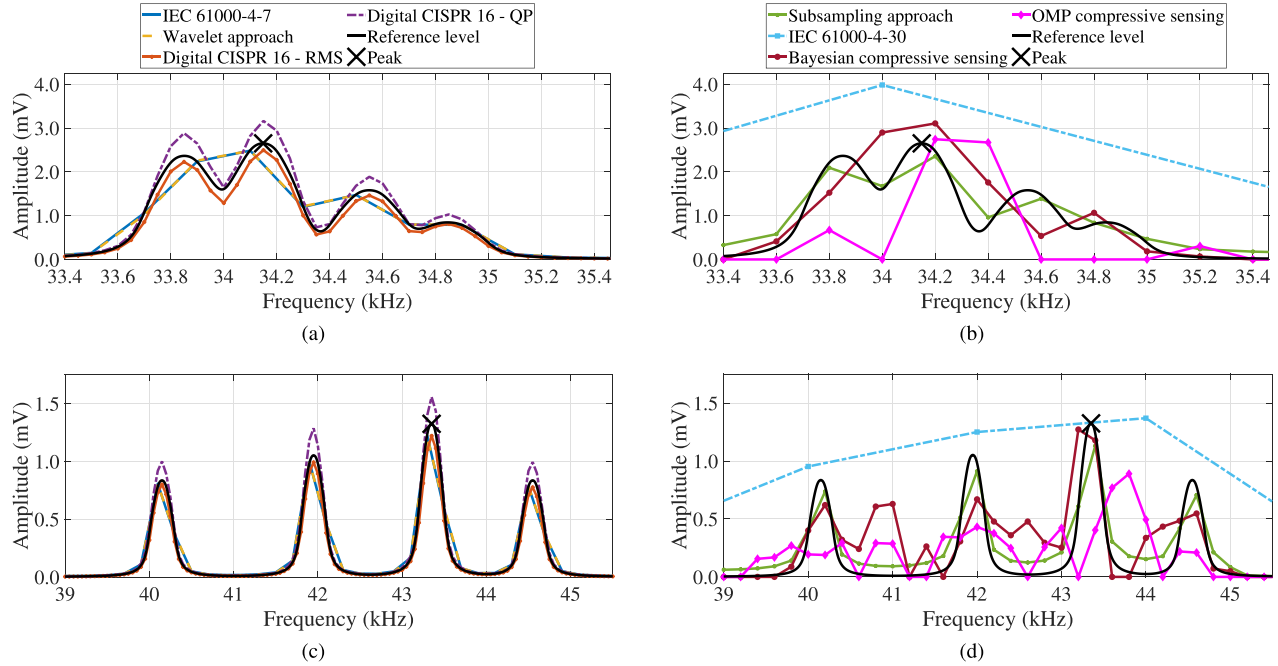[1] Integral values were calculated over the frequency range 2 kHz to 150 kHz

Fig. 6. Spectral amplitude results for the synthetic signal with several narrowband emissions (test signal B). Results have been divided between four figures for visual clarity. (a) Results in the frequency range 33.4–35.4 kHz for the IEC 61000-4-7 method, wavelet approach, and Digital CISPR 16 method. (b) Results in the frequency range 33.4–35.4 kHz for the subsampling approach, IEC 61000-4-30 method, and compressive sensing methods. (c) Results in the frequency range 39–45.5 kHz for the IEC 61000-4-7 method, wavelet approach, and Digital CISPR 16 method. (d) Results in the frequency range 39–45.5 kHz for the subsampling approach, IEC 61000-4-30 method, and compressive sensing methods.

TABLE IV
ERRORS IN RESULTS FOR NARROWBAND EMISSIONS (TEST SIGNAL C)

Frequency range	33-36 kHz		39-46 kHz	
Error in peak values	$E_{f,P}$ (Hz)	$E_{U,P}$ (%)	$E_{f,P}$ (Hz)	$E_{U,P}$ (%)
IEC 61000-4-7	-	−6.3	-	−7.9
Wavelet approach	-	−6.4	-	−8.6
Digital CISPR 16 - RMS	-	−5.9	-	−7.8
Subsampling approach	-	−11.1	-	−14.6
IEC 61000-4-30	-	50.3	-	3.4
Bayesian compressive sensing	-	17.2	−150	−4.0
OMP compressive sensing	-	3.5	450	−32.8
Reference	34 149		43 350	

and the subsampling approach in Fig. 6(d) match the four spectral peaks of the reference spectrum.

Table IV shows that IEC 61000-4-7, wavelet approach, and digital CISPR 16 method are within 10% of the peak reference values, while the subsampling approach has greater deviations. The IEC 61000-4-30 and compressive sensing methods have deviations within 10% only for one peak value.

Fig. 6(b) and (d) shows that the IEC 61000-4-30 method does not resolve the emissions, while the compressive sensing methods result in spectra with different shapes from the reference level in terms of number, width, and location of identified emissions.

D. Synthetic Grid Signal—Test Signal D

The results for synthetic test signals B and C have revealed various emission characteristics that cause the accuracy of the methods to deviate from the calibration scenario. Test signal D has been designed to assess the performance of the methods in a grid measurement scenario.

Fig. 7 shows the plots of the spectral amplitude results for the synthetic grid signal. Similar to the results of the grid recording in Fig. 5, it can be observed that the amplitude spectra of the IEC 61000-4-7 method and wavelet approach overlap, with the digital CISPR 16 rms values slightly lower and quasi-peak values higher. Further similarities to measured signal results are the sparsity of the Bayesian compressive sensing above 90 kHz and the amplitude values for the compressive sensing methods that have not been resolved
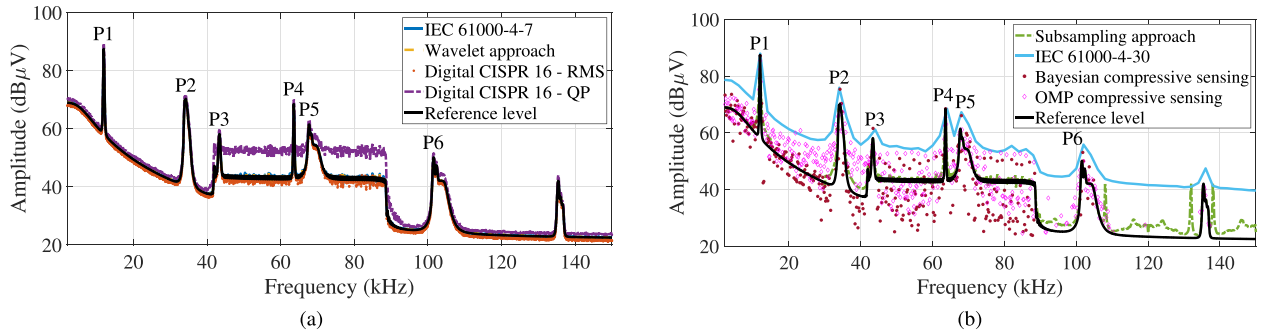
Fig. 7.   Spectral amplitude results for the synthetic grid signal (test signal D). Results have been divided between two figures for visual clarity.

TABLE V
ERRORS IN RESULTS FOR THE SYNTHETIC GRID SIGNAL (TEST SIGNAL D)

	Error in frequency and amplitude of peak narrowband emissions												Error in integral values	
	$E_{f,P1}$ (Hz)	$E_{U,P1}$ (%)	$E_{f,P2}$ (Hz)	$E_{U,P2}$ (%)	$E_{f,P3}$ (Hz)	$E_{U,P3}$ (%)	$E_{f,P4}$ (Hz)	$E_{U,P4}$ (%)	$E_{f,P5}$ (Hz)	$E_{U,P5}$ (%)	$E_{f,P6}$ (Hz)	$E_{U,P6}$ (%)	40-90 kHz E_T (%)	2-150 kHz E_T (%)
IEC 61000-4-7	-	−1.1	-	−3.7	-	1.3	-	−10.5	-	0.7	-	0.0	0.5	0.8
Wavelet approach	-	−1.2	-	−3.8	-	1.0	-	−11.1	-	0.7	-	0.2	0.6	0.9
Digital CISPR 16 - RMS	-	−6.3	-	−12.2	-	−9.5	-	−5.9	-	−9.6	-	−8.2	-	-
Subsampling approach	-	−19.0	-	−3.9	-	−4.9	-	−7.3	-	−6.0	-	−1.9	1.6	0.6
IEC 61000-4-30	-	5.8	-	91.4	-	41.6	-	0.5	-	95.2	-	93.6	2.4	2.9
Bayesian compressive sensing	-	−2.9	-	80.0	-	48.5	-	0.5	284	69.9	245	41.0	−4.2	1.3
OMP compressive sensing	-	−20.6	205	−4.0	-	−20.4	-	−28.8	484	−3.9	445	−2.5	8.8	4.9
Reference	11 930		34 195		43 353		63 570		67 716		101 555			

effectively to the 200-Hz level. However, the use of a synthetic signal has the advantage of known reference levels, which means that reliable conclusions about the accuracy of the results can be drawn.

It can be seen clearly that the compressive sensing methods trace the reference spectrum less closely. The amplitude spectrum given by the subsampling approach matches the reference level well although, above 108 kHz, some additional narrowband emissions can be observed.

Table V gives errors in frequency and amplitude values identified for the highest peak narrowband emissions, as well as errors in integral values for the PLC range and over 2–150 kHz. The error values confirm that the IEC 61000-4-7 method and the wavelet approach are closest to the reference level for all but one of the peak amplitude values, and the frequency values are accurate to within the 200-Hz step between center frequencies. The subsampling method gives the results between 3.9% and 19% below the reference peak amplitudes but the smallest deviation of 0.6% from the integral value over the whole frequency range. The performance of the compressive sensing methods is mixed. For some narrowband emissions, the methods successfully decrease the frequency step from 2 kHz to 200 Hz, thereby reducing the error in amplitude (e.g., $E_{U,P2}$, $E_{U,P5}$, and $E_{U,P6}$) compared with the IEC 61000-4-30 results. However, this performance is not consistent; for some peaks, the amplitude error is, in fact, increased. All methods give integral values of this synthetic grid signal within 10% of the reference values.

VI. DISCUSSION

A. Accuracy of Methods

In the previous section, results of the application of different measurement methods proposed for grid emission measurements in the range 2–150 kHz have been analyzed. The motivation for the analysis was to investigate the existence and extent of differences between results and to make an overall accuracy assessment.

For the tested signals and features, the IEC 61000-4-7 method and the wavelet approach have demonstrated the highest accuracy for peak amplitude values of narrowband emissions, as well as integral values. Depending on the required tolerance for reproducibility, the results of these two methods could be considered equivalent.

The digital CISPR 16 method gave lower rms amplitude values, which can be expected because the frequency response of each bin is attenuated to −6 dB at a bandwidth of 200 Hz, while the reference level defined in this study is based on flat frequency response. Due to a frequency step of 50 Hz, the frequency of some peak narrowband emissions and the shape of the amplitude spectrum were identified more accurately than other methods. The method provides also quasi-peak values, which may be used for direct comparability with laboratory emission measurements of appliances and compatibility levels. By definition, the quasi-peak values are equal to rms values for constant signals, such as test signal B in this study. However, for time-varying emissions, the quasi-peak does not reflect signal power. The quasi-peak values are driven by the maximum emissions level and can, therefore, be significantly higher than rms values.

For the subsampling approach, deviations from the reference levels have fluctuated, mostly exceeding those of the IEC 61000-4-7 method and wavelet approach, but in some instances being lower than for CISPR 16 rms values. The overall accuracy of the subsampling approach is influenced by the attenuation of the analog filters, and the results have shown that some high-amplitude narrowband emissions at

lower frequencies can appear as images in the higher frequency bands with amplitude levels similar to the actual emissions.

The IEC 61000-4-30 method has higher amplitude values relative to reference levels defined for a 200-Hz bandwidth, which is expected for a method with 2-kHz bins, but integral values have been accurate to within 5%. In this comparison, two other methods have been included, which are designed to decrease the frequency step from 2 kHz to 200 Hz, while maintaining a short measurement interval of 0.5 ms. In some instances, these methods have reduced errors in the frequency and amplitude of peak narrowband emissions; however, the improvement in accuracy was not consistently achieved.

B. Toward a Normative Method

To limit the scope of this study, the focus has been on comparing the accuracy of aggregated rms results of different proposed methods. A further aspect to investigate is the capability of the methods to accurately identify and represent time variation of emissions. While rms values can provide an indication of additional thermal stress caused by emissions, duration and rate of occurrence may be needed to characterize other interference phenomena [27].

The primary consideration in the design of a measurement method for 2–150-kHz emissions should be to meet the requirements of the relevant normative standard, which are due to be specified in the next edition of IEC 61000-4-30 Annex C. The normative specification is expected to set requirements for bandwidth (likely 200 Hz), measurement time, accuracy, output quantities, such as rms or quasi-peak values, and aggregation over time and frequency. Compliance of any designed method with the normative specifications will ensure comparability and reproducibility between instruments from different manufacturers.

Furthermore, the computational resources needed by a method must be assessed to determine if the real-time implementation is possible on a typical power quality instrument and the extent of additional manufacturing costs. A comprehensive assessment must take into account the total number of elementary operations, memory requirements, the scope for parallel processing, and hardware suitability.

The development of a normative method specification is still in progress, and it is a complex task since competing for desirable requirements, including accuracy in frequency, amplitude and integral values, time and frequency resolutions, comparability to compatibility levels, ease, and cost of implementation must be balanced. The authors believe that no single method can fulfill all requirements optimally; therefore, compromises must be made, or the normative specification could include more than one method for different measurement objectives.

VII. CONCLUSION

This article presents a comparative analysis of the accuracy of a range of measurement methods for LV grid emissions in the range 2–150 kHz. In contrast to previous comparisons, new methods based on alternative concepts not currently considered by standards relevant to this frequency range have been included. Significant differences in results were identified using a real grid measurement, and the accuracy of each method was assessed using synthetic signals with known frequency content, including a grid emulation containing several typical emissions. It was shown that a method based on wavelet decomposition can achieve the same level of accuracy as the method for 2–9 kHz in informative Annex B of IEC 61000-4-7. The potential of compressive sensing for increased frequency resolution without loss of time resolution was demonstrated, but such methods require further development to ensure consistent levels of accuracy for different types of emission.

This article contributes to the evaluation of different candidate methods to provide a knowledge base for the definition of a normative grid measurement method for 2–150-kHz emissions, which is one of the missing elements to ensure coordination of EMC in resilient future power networks with a high penetration of communication technologies and power electronic devices.

REFERENCES

[1] C. CIGRE/CIRED JWG, "Power quality and EMC issues with future electricity networks," in *Proc. CIGRE*, Mar. 2018, pp. 1–5.

[2] M. H. J. Bollen *et al.*, "Power quality concerns in implementing smart distribution-grid applications," *IEEE Trans. Smart Grid*, vol. 8, no. 1, pp. 391–399, Jan. 2017.

[3] X. Liang, "Emerging power quality challenges due to integration of renewable energy sources," *IEEE Trans. Ind. Appl.*, vol. 53, no. 2, pp. 855–866, Mar. 2017.

[4] I. Fernández, D. de la Vega, A. Arrinda, I. Angulo, N. Uribe-Pérez, and A. Llano, "Field trials for the characterization of non-intentional emissions at low-voltage grid in the frequency range assigned to NB-PLC technologies," *Electronics*, vol. 8, no. 9, p. 1044, Sep. 2019.

[5] S. K. Rönnberg *et al.*, "On waveform distortion in the frequency range of 2 kHz-150 kHz—Review and research challenges," *Electr. Power Syst. Res.*, vol. 150, pp. 1–10, Sep. 2017.

[6] *Electromagnetic Compatibility (EMC)—Part 4-7: Testing and Measurement Techniques General Guide on Harmonics and Interharmonics Measurements and Instrumentation, for Power Supply Systems and Equipment Connected Thereto*, document IEC 61000-4-7:2002+AMD1, 2008.

[7] *Electromagnetic Compatibility (EMC)—Part 4-30: Testing and Measurement Techniques Power Quality Measurement Methods*, document IEC 61000-4-30 Ed.3, 2015.

[8] *Specification for Radio Disturbance and Immunity Measuring Apparatus and Methods—Part 1-1: Radio Disturbance and Immunity Measuring Apparatus—Measuring Apparatus*, document CISPR 16-1-1:2019, 2019.

[9] M. Klatt, J. Meyer, and P. Schegner, "Comparison of measurement methods for the frequency range of 2 kHz to 150 kHz," in *Proc. 16th Int. Conf. Harmon. Qual. Power (ICHQP)*, May 2014, pp. 818–822.

[10] A. Grevener, J. Meyer, and S. K. Rönnberg, "Comparison of measurement methods for the frequency range of 2–150 kHz (supraharmonics)," in *Proc. IEEE Int. Workshop Appl. Meas. Power Syst. (AMPS)*, Bologna, Italy, 2018, pp. 1–5.

[11] T. M. Mendes, C. A. Duque, L. R. Manso da Silva, D. D. Ferreira, J. Meyer, and P. F. Ribeiro, "Comparative analysis of the measurement methods for the suparharmonic range," *Int. J. Electr. Power Energy Syst.*, vol. 118, Jun. 2020, Art. no. 105801.

[12] V. Khokhlov, J. Meyer, A. Grevener, T. Busatto, and S. Ronnberg, "Comparison of measurement methods for the frequency range 2–150 kHz (Supraharmonics) based on the present standards framework," *IEEE Access*, vol. 8, pp. 77618–77630, 2020.

[13] T. M. Mendes, C. A. Duque, L. R. M. Silva, D. D. Ferreira, and J. Meyer, "Supraharmonic analysis by filter bank and compressive sensing," *Electric Power Syst. Res.*, vol. 169, pp. 105–114, Apr. 2019.

[14] S. Zhuang, W. Zhao, R. Wang, Q. Wang, and S. Huang, "New measurement algorithm for supraharmonics based on multiple measurement vectors model and orthogonal matching pursuit," *IEEE Trans. Instrum. Meas.*, vol. 68, no. 6, pp. 1671–1679, Jun. 2019.

[15] S. Zhuang, W. Zhao, Q. Wang, Z. Wang, L. Chen, and S. Huang, "A high-resolution algorithm for supraharmonic analysis based on multiple measurement vectors and Bayesian compressive sensing," *Energies*, vol. 12, no. 13, p. 2559, Jul. 2019.

[16] S. Lodetti, J. Bruna, J. J. Melero, V. Khokhlov, and J. Meyer, "A robust wavelet-based hybrid method for the simultaneous measurement of harmonic and supraharmonic distortion," *IEEE Trans. Instrum. Meas.*, vol. 69, no. 9, pp. 6704–6712, Sep. 2020.

[17] A. J. Collin, S. Z. Djokic, J. Drapela, R. Langella, and A. Testa, "Proposal of a desynchronized processing technique for assessing high-frequency distortion in power systems," *IEEE Trans. Instrum. Meas.*, vol. 68, no. 10, pp. 3883–3891, Oct. 2019.

[18] P. Wright, D. Ritzmann, J. Meyer, V. Khokhlov, D. De La Vega, and I. Fernandez, "Measurement methods comparison in the frequency range 2–150 kHz," in *Conf. Precis. Electromagn. Meas. (CPEM)*, 2020, p. 5.

[19] *Electromagnetic compatibility (EMC)—Environment—Compatibility Levels for Low-Frequency Conducted Disturbances and Signalling in Public Low-Voltage Power Supply Systems*, document IEC 61000-2-2:2002+AMD1, 2018.

[20] M. Schwenke and D. Klingbeil, "Application aspects and measurement methods in the frequency range from 9 kHz to 150 kHz," in *Proc. 25th Int. Conf. Electr. Distrib. (CIRED)*, Madrid, India, 2019, pp. 1–8.

[21] F. Krug and P. Russer, "Quasi-peak detector model for a time-domain measurement system," *IEEE Trans. Electromagn. Compat.*, vol. 47, no. 2, pp. 320–326, May 2005.

[22] I. Fernandez *et al.*, "Characterization of non-intentional emissions from distributed energy resources up to 500 kHz: A case study in spain," *Int. J. Electr. Power Energy Syst.*, vol. 105, pp. 549–563, Feb. 2019.

[23] G. F. Bartak and A. Abart, "EMI of emissions in the frequency range 2 kHz–150 kHz," in *Proc. 22nd Int. Conf. Exhib. Electr. Distrib.*, 2013, p. 1271.

[24] *Narrowband Orthogonal Frequency Division Multiplexing Power Line Communication Transceivers for PRIME Networks*, document ITU-T G.9904, 2012.

[25] *Investigation Results on Electromagnetic Interference in the Frequency Range below 150 kHz*, document CLC/TR 50669, 2017.

[26] I. Fernández, M. Alberro, J. Montalbán, A. Arrinda, I. Angulo, and D. de la Vega, "A new voltage probe with improved performance at the 10 kHz–500 kHz frequency range for field measurements in LV networks," *Measurement*, vol. 145, pp. 519–524, Oct. 2019.

[27] V. Khokhlov, J. Meyer, P. Schegner, D. Agudelo-martinez, and A. Pavas, "Immunity assessment of household appliances in the frequency range from 2 to 150 kHz," in *Proc. 25th Int. Conf. Electr. Distrib. (CIRED)*, Madrid, India, 2019, pp. 1–5.

Deborah Ritzmann received the B.Sc. degree in mathematics and physics from University College London, London, U.K., in 2012, and the Ph.D. degree in electronic engineering from the University of Reading, Reading, U.K., in 2017.

She subsequently worked for National Grid ESO and renewable generation developer Anesco. She joined the National Physical Laboratory, U.K., in 2019, where she is currently a Higher Research Scientist contributing to research projects in the field of electricity networks metrology.

Stefano Lodetti (Member, IEEE) received the B.Sc. and M.Sc. degrees in physics from the University of Milan, Milan, Italy, in 2012 and 2015, respectively, and the M.Sc. degree in renewable energies and energy efficiency from the University of Zaragoza, Zaragoza, Spain, in 2018.

From 2016 to 2019, he was a Researcher with Fundación CIRCE, Spain. Since 2020, he has been a Higher Research Scientist with the National Physical Laboratory, Teddington, U.K. His research interests are power systems measurements and power quality.

David de la Vega (Senior Member, IEEE) received the M.Sc. and Ph.D. degrees in telecommunication engineering from the University of the Basque Country (UPV/EHU), Spain, in 1996 and 2008, respectively.

He is currently an Associate Professor with the Department of Communications Engineering, UPV/EHU. His current research is focused on the analysis of signal propagation and the effects of interferences on smart grids' communications.

Victor Khokhlov (Member, IEEE) received the B.Sc. degree in electrical power engineering from the Moscow Power Engineering Institute, Moscow, Russia, in 2014, and the M.Sc. degree in electrical power engineering from the Ilmenau University of Technology, Ilmenau, Germany, in 2017. He is currently pursuing the Ph.D. degree in electrical power engineering with the Institute of Electrical Power Systems and High Voltage Engineering, Technische Universität Dresden, Dresden, Germany.

His research interests include different aspects of network disturbances above 2 kHz, especially their impact on functionality and lifetime of modern electrical appliances.

Alexander Gallarreta received the B.Sc. degree in telecommunications technologies engineering from the University of the Basque Country (UPV/EHU), Spain, in 2019, where he is currently pursuing the M.Sc. degree in telecommunications engineering.

He works as a Research Student with UPV/EHU. His research is focused on signal processing for the analysis of low-voltage grid emissions measurement methods.

Paul Wright received the B.Sc. and Ph.D. degrees in electrical and electronic engineering from the University of Surrey, Surrey, U.K., in 1987 and 2002, respectively.

He spent three years as a Research Fellow with the University of Surrey, where he was involved in the field of spacecraft sensors and attitude control. This was followed by three years with the Central Electricity Research Laboratory, where he was involved in advanced control systems. In 1992, he joined the National Physical Laboratory, Teddington, U.K., where he is currently a Principal Research Scientist specializing in ac measurements and waveform analysis. He has coordinated five EU collaborative research and development projects and he is currently a Coordinator of the EU project on 2–150-kHz grid measurement SupraEMI of which this work is part.

Jan Meyer (Senior Member, IEEE) received the Dipl.Ing. and Dr. Ing. degrees in electrical power engineering and the Habilitation degree in power quality from Technische Universität Dresden, Dresden, Germany, in 1994, 2004, and 2018, respectively.

He is currently a Senior Lecturer and the Leader of the Power Quality Research Team, Technische Universität Dresden. His research interests include network disturbances and their assessment, especially distortion below and above 2 kHz, the accuracy of power quality measurements, and big data analysis techniques applied to power quality data.

Dr. Meyer is a member of several national and international working groups on EMC standardization and several CIGRE working groups and the CIRED Technical Committee.

Igor Fernández received the M.Sc. and Ph.D. degrees in telecommunication engineering from the University of the Basque Country (UPV/EHU), Spain, in 2001 and 2011, respectively.

He is currently an Assistant Professor with the Department of Communications Engineering, UPV/EHU. His current research interests focus on new digital broadcasting technologies and power line communications (PLC).

Dimitrij Klingbeil received the diploma degree in computer science from the Technical University of Berlin (TU Berlin), Berlin, Germany, in 2008.

He is currently a Senior Hardware Developer with Siemens AG, Berlin. His professional interests include measurement methods and techniques in power systems and power quality.